

Figure S1. Cardiomyocytes and CD90+ stromal cells remain transcriptionally distinct following CHIR treatment.

3D PCoA analysis of CHIR or DMSO treated 2D derived cardiomyocytes and CD90+ stromal cells. n = 3 for all groups. Red = cardiomyocytes, Orange = CD90+ stromal cells

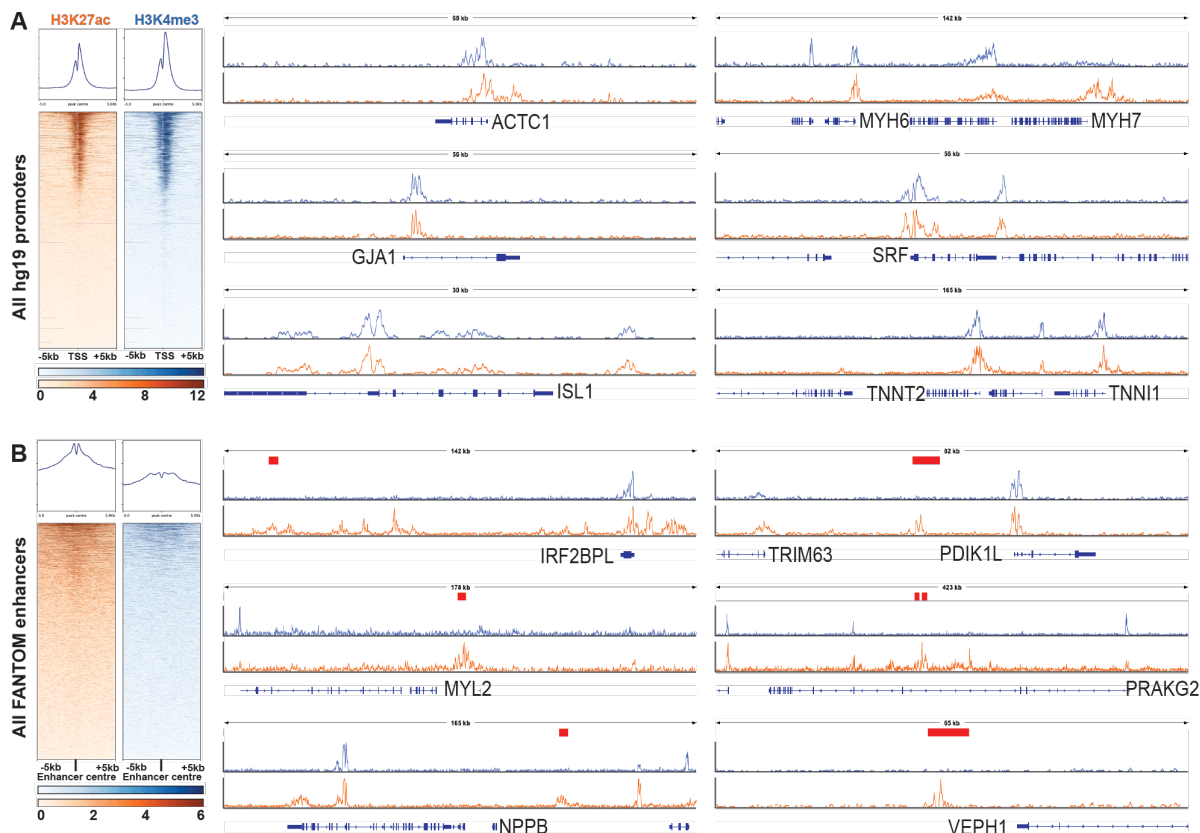


Figure S2. H3K4me3 and H3K27ac peaks at well-characterised cardiomyocyte-specific promoters and enhancers

(A) Left panel displays a heatmap of ChIP-seq H3K4me3 and H3K27ac peaks ± 5 kb from all promoters annotated in the hg19 genome assembly. H3K4me3 and H3K27ac peaks surrounding cardiomyocyte-related genes. (B) Left panel is a heatmap of H3K4me3 and H3K27ac heatmaps at all enhancers identified by the FANTOM consortium (Arner et al., 2015). Right panel displays genome tracks surrounding known cardiomyocyte genes. Red bars indicate validated human cardiac enhancer sites (Spurrell et al., 2019; Visel et al., 2009). Blue = H3K4me3, Orange = H3K27ac

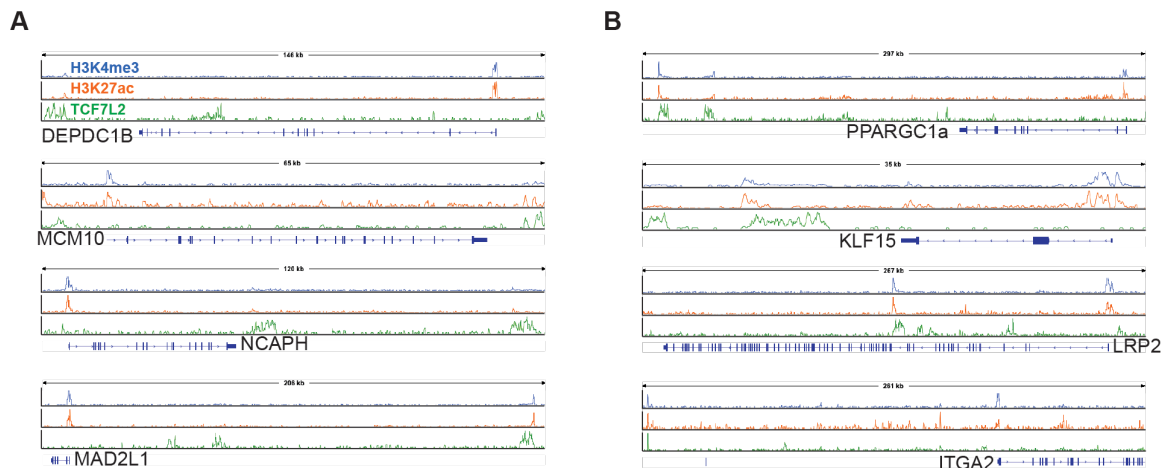


Figure S3. Proximal and distal localisation of TCF7L2 to CHIR-regulated genes

Genome tracks surrounding CHIR-regulated direct targets of TCF7L2 in 2D derived human cardiomyocytes. H3K4me3, H3K27ac, and TCF7L2 ChIP-seq peaks are displayed in blue, orange and green, respectively.

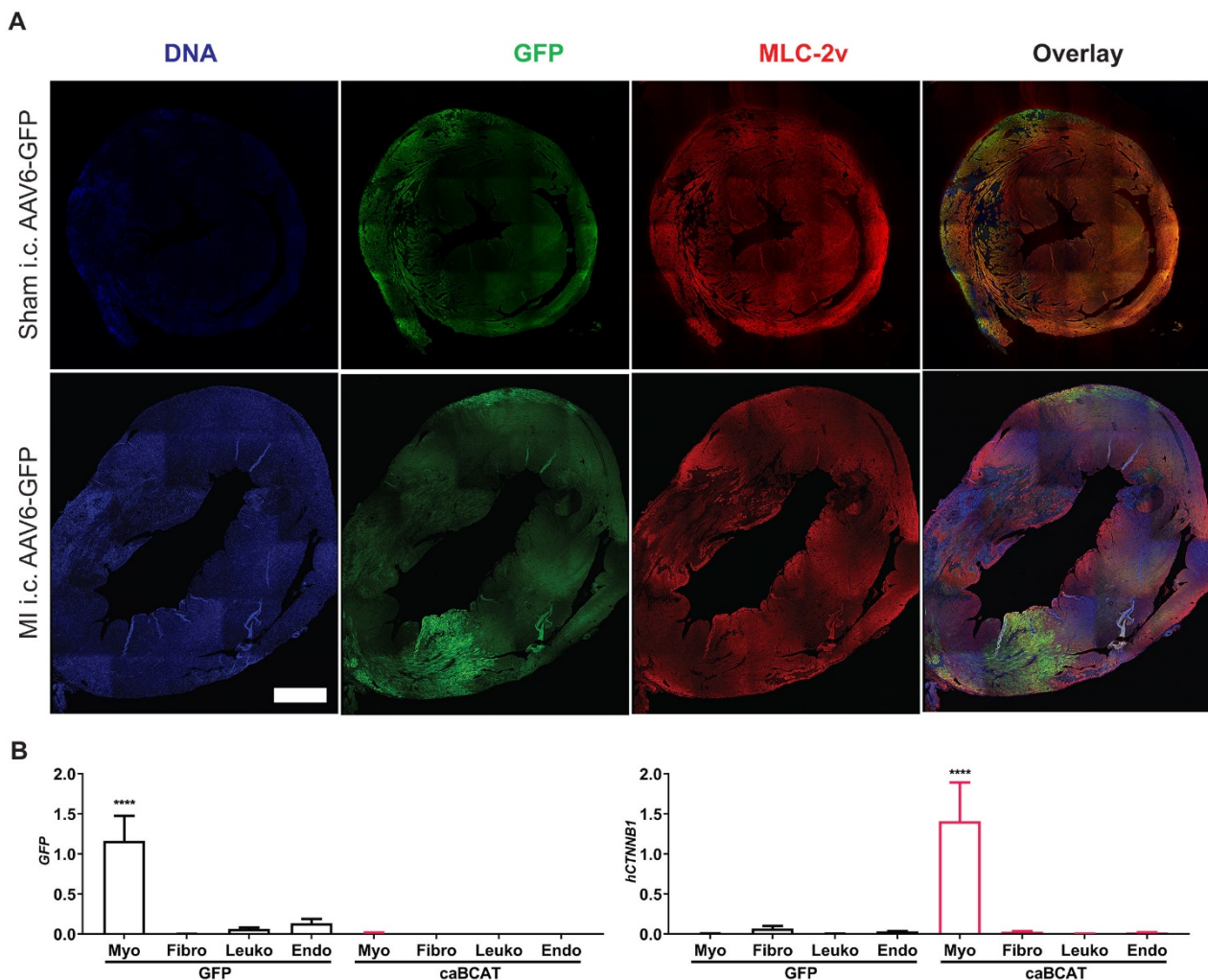


Figure S4. AAV6 delivered constructs are specifically expressed in border zone cardiomyocytes following intracardiac injection in mice.

(A) Confocal tile scan images of AAV6-GFP injected hearts following Sham or MI surgery. Each heart was injected with 1×10^{11} viral particles at 4 sites surrounding the infarct. Representative images shown. Images taken 3 days post-surgery and intracardiac injections. Scale bar = 1 mm. (B) qPCR for human *CTNNNB1* and GFP in cardiomyocytes, fibroblasts, leukocytes and endothelial cells isolated 3 days post AAV6-GFP and AAV6-caBCAT injection. $n = 4$.

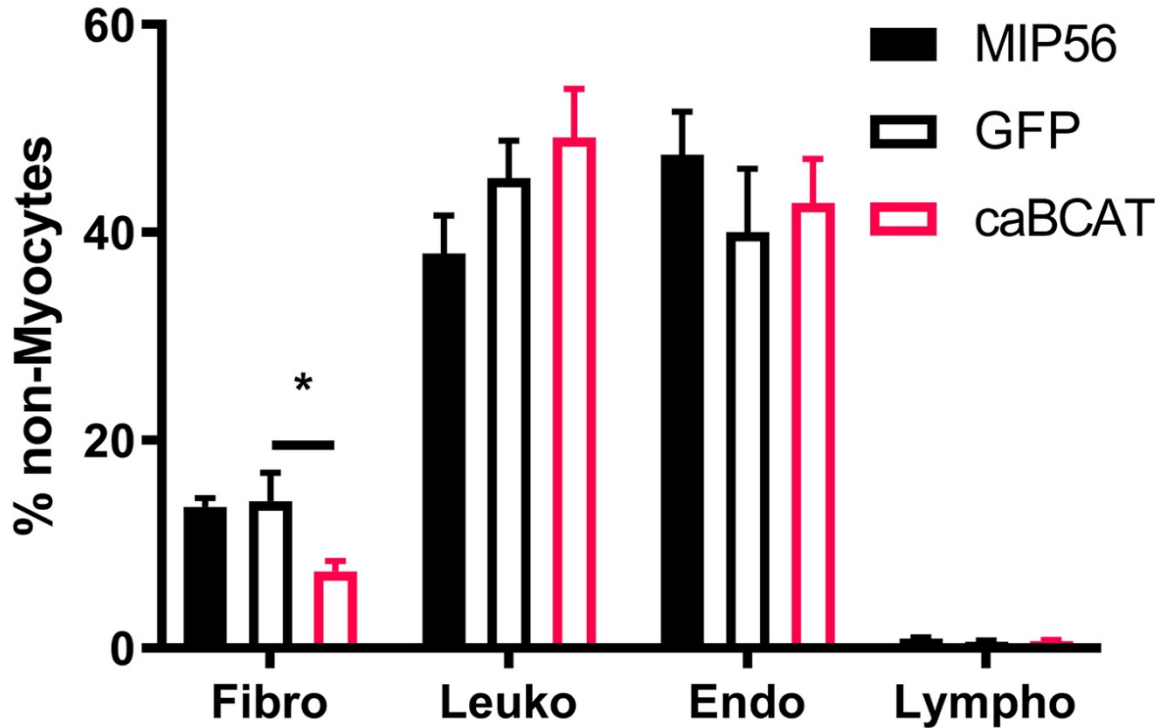


Figure S5. Fibroblast number is reduced in caBCAT treated hearts at day 3 post MI.

Fibroblasts, leukocytes endothelial cells and lymphatic endothelial cells well isolated from MIP56 (no i.c. injection), AAV6-GFP and AAV-caBCAT injected hearts at day 3 post MI. The fibroblast population was diminished in caBCAT treated hearts. n = 4.

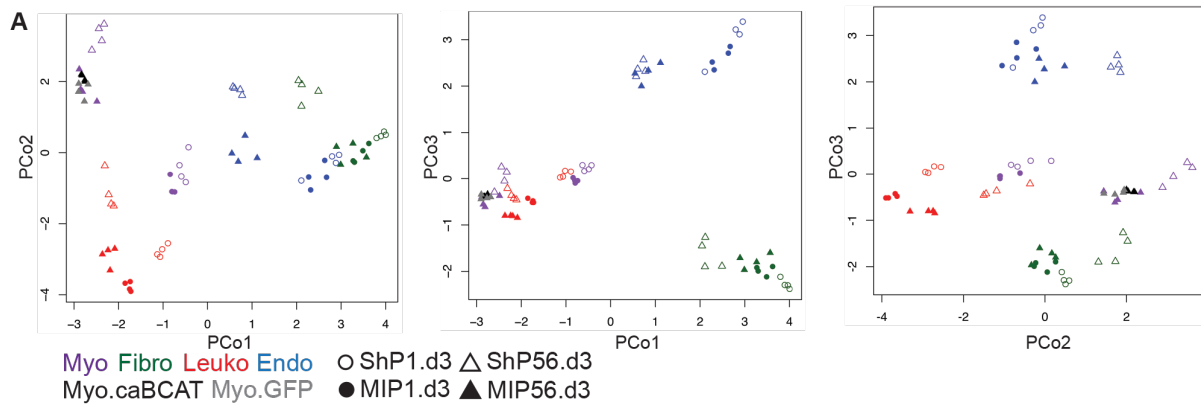


Figure S6. The transcriptional identity of adult cardiomyocytes is unaltered by caBCAT

3D principal coordinate analysis (PCoA) comparing MIP56.d3 caBCAT or GFP treated cardiomyocytes and the entire multicellular RNA-seq dataset (Quaife-Ryan et al., 2017). n = 4 for all groups. Purple = MIP56.d3 cardiomyocytes, green = MIP56.d3 fibroblasts, red = MIP56.d3 leukocytes, blue = MIP56.d3 endothelial cells, black = MIP56.d3 caBCAT cardiomyocytes and gray = MIP56.d3 GFP cardiomyocytes. Open circles = ShP1.d3, closed circles = MIP1.d3, open triangles = ShP56.d3, closed triangles = MIP56.d3.

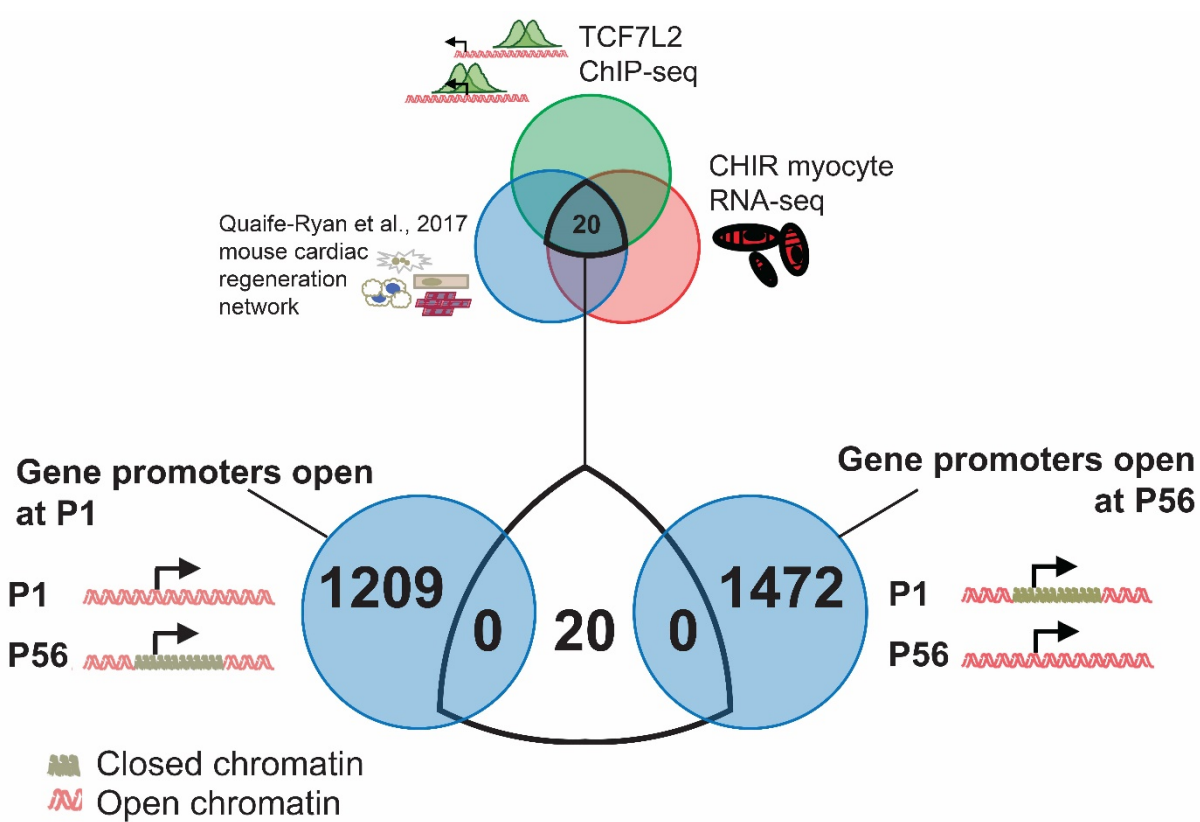


Figure S7. β -catenin target gene promoters are not epigenetically repressed during postnatal cardiomyocyte maturation

The 20 β -catenin immature myocyte target genes identified in Fig. 6 were intersected with P1 and P56 ATAC-seq cardiomyocyte datasets. Chromatin accessibility was unaltered around these target gene promoters during cardiomyocyte development. ATAC-seq datasets obtained from (Quaife-Ryan et al., 2017) (GSE95764). For each ATAC-seq, n = 3.

Table S1. Antibodies used in this study

Antibody	Species	Samples	Company	Cat No	Dilution
Alexa Fluor 488 goat anti-chicken IgG (H+L)	Goat IgG	Secondary antibody	Life Technologies	A-11039	1:33
Alexa Fluor 488 goat anti-mouse IgG (H+L)	Goat IgG	Secondary antibody	Life Technologies	A-11029	1:10
Alexa Fluor 488 goat anti-mouse IgM (μ chain)	Goat IgG	Secondary antibody	Life Technologies	A-21042	1:33
Alexa Fluor 488 goat anti-rabbit IgG (H+L)	Goat IgG	Secondary antibody	Life Technologies	A-11034	1:67
Alexa Fluor 555 goat anti-mouse IgG (H+L)	Goat IgG	Secondary antibody	Life Technologies	A-21422	1:100
Alexa Fluor 555 goat anti-rabbit IgG (H+L)	Goat IgG	Secondary antibody	Life Technologies	A-21428	1:100
Alexa Fluor 633 goat anti-rabbit IgG (H+L)	Goat IgG	Secondary antibody	Life Technologies	A-21070	1:100
anti-BrdU	IgG1, kappa light chain	IF imaging	DSHB	G3G4 (anti-BrdU)	1:100
Anti-MLC-2v	Rabbit IgG	IF imaging	Proteintech	10906-1-AP	1:1000
Anti-phospho-Histone H3 (Ser10)	Rabbit polyclonal	IF imaging	Millipore	06-570	1:100
Anti-TnTc	Mouse IgG1	IF imaging	Thermo Scientific	MS-295-P0	1:100
anti-β-catenin (PY489)	Mouse IgM	IF imaging	DSHB	PY489-B-catenin	1:400
CD31-BV421	Rat IgG2a	Mouse FACS	BioLegend	102423	1:100
CD45-FITC	Rat IgG2b	Mouse FACS	Miltenyi Biotec	130-102-778	1:200
CD90	Mouse IgG2A	hPSC FACS	RnD Systems	MAB2067	1:400
CD90-APC	Rat IgG2c	Mouse FACS	ThermoFisher	A14727	1:400
GFP	Chicken polyclonal	IF imaging	Abcam	ab13970	1:400
Ki-67 (D3B5)	Rabbit IgG	IF imaging	Cell Signalling Technology	9129	1:400
Podoplanin-PE/Cy7	Syrian Hamster IgG	Mouse FACS	BioLegend	127411	1:400
Wheat germ agglutinin, Alexa Fluor 488	NA	IF imaging	ThermoFisher Scientific	W11261	1:400
α-Actinin (clone EA-53)	Mouse IgG1	IF imaging	ThermoFisher	A-21070	1:400

Table S2 Primers for quantitative PCR

Gene	Accession	Forward	Reverse	Size (bp)
Human qPCR primers				
18s	18s repeat sequence	TCGAGGCCCTGTAATTGGAA	CCCTCCAATGGATCCTCGTT	61
COL1a1	ENSG00000108821	GTGCTAACGGTGCCAATGGT	ACCAGGTTCACCGCTGTTAC	128
HPRT1	ENSG00000165704	AACCTCTCGGCTTCCCCG	TCACTAATCACGACGCCAGG	150
MYH6	ENSG00000197616	CTCCTCCTACGCAACTGC	ACACCGTCTGGAAGGATGA	83
CTNNB1	ENSG00000168036	CTTACACCCACCATCCACT	TGATGTGCACGAACAAGCAA	144
Mouse qPCR primers				
18s	18s repeat sequence	TCGAGGCCCTGTAATTGGAA	CCCTCCAATGGATCCTCGTT	61
Anln	ENSMUSG0000036777	ATGTTAGTGGCTTGGTGCC	TGGGATTCTTCGCCTCTCA	102
Birc5	ENSMUSG0000017716	AACCCGATGACAACCCGAT	TGGTCTCCTTGCAATTGGTTC	150
Cdk1	ENSMUSG0000019942	ACACACACGAGGTAGTGACG	AACCGGAGTGGAGTAACGAG	80
Depdc1b	ENSMUSG0000021697	TTGTGATTCAAAC TGCGGCG	TCCACTGTTCATTCACAGC	143
E2f1	ENSMUSG0000027490	ACCCAGGGAAAGGTGTGAAA	CAAGAACGCTTGGTGGTCA	80
Hprt	ENSMUSG0000025630	AGGCCAGACTTGTGGATTGAA	CAACTTGCGCTCATCTTAGGCTT	150
Iqgap3	ENSMUSG0000028068	GAGCTCGGACAGCCTATGAGC	AGCCGGCAGAGGTACTGATA	88
Kif18a	ENSMUSG0000027115	GTGGATTGCCAACGCATT	TTTATAGCCCACTTCAGTCTGT	80
Kif4	ENSMUSG0000034311	CCAGCAAACAGAAACCCAT	AAGGTTGGGCTTAGGTGGA	87
Klf15	ENSMUSG0000030087	GGAGAGCGGGGAGAGC	TGTGGTACTGGACTCCG	148
Mad2l1	ENSMUSG0000029910	GAAGAATCGGACCGCAA	CAGACCAACGAACCGTCTC	138
Plk4	ENSMUSG0000025758	CGTAGAGAAGGCGTCCTGAT	TAAAGTCCTCGATCCTCTCCC	143
Ppargc1a	ENSMUSG0000029167	CTCTCAGTAAGGGCTGGTT	CAGCACACTTATGTCACTCC	150
Ptg1	ENSMUSG0000020415	TGGCGCAGTCTCGAGTAAT	ATCCTTAGATGCCAACCGC	91
Miscellaneous qPCR Primers				
GFP	-	AAGGGCATCGACTTCAAGG	TGCTTGCGGCCATGATATAG	95

Table S3 Summary of RNA-seq mapping efficiencies of MIP56 caBCAT experiment

Sample	number of reads	%uniquely mapped reads	%multi-mapped reads	%unmapped
Myo_GFP_1	65812645	71.21%	25.52%	3.27%
Myo_GFP_2	58613420	69.79%	26.80%	3.41%
Myo_GFP_3	67027367	71.61%	24.98%	3.41%
Myo_GFP_4	65004587	71.52%	24.60%	3.88%
Myo_BCAT_1	71693147	71.26%	25.37%	3.37%
Myo_BCAT_2	74057324	73.35%	23.83%	2.82%
Myo_BCAT_3	67597492	70.32%	26.50%	3.18%
Myo_BCAT_4	65687633	69.98%	26.81%	3.21%

Table S4 Summary of mapping efficiencies for ChIP-seq

Sample	number of reads	%uniquely mapped reads	%multi-mapped reads	%unmapped
H3K27ac_1	40192146	69.93%	28.52%	1.55%
H3K27ac_2	73153197	76.80%	22.26%	0.94%
H3K4me3_1	42817370	67.22%	31.03%	1.74%
H3K4me3_2	71856079	75.62%	22.83%	1.54%
Input_1	82802143	71.20%	27.28%	1.53%
Input_2	85319259	73.57%	24.84%	1.59%
TCF7I2_1	66744568	68.12%	29.74%	2.09%
TCF7I2_2	77627877	68.35%	28.43%	3.22%

Table S5. Bioinformatic programs used in this study

Software	Reference	RRID
NCBI Primer-BLAST	(Ye et al., 2012)	RRID:SCR_003095
Trimmomatic	(Bolger et al., 2014)	RRID:SCR_011848
STAR	(Dobin et al., 2013)	RRID:SCR_015899
HTSeq-count	(Anders et al., 2015)	RRID:SCR_011867
EdgeR	(Robinson et al., 2010)	RRID:SCR_012802
DAVID	(Huang et al., 2007)	RRID:SCR_001881
GENE-E	Broad Institute	N/A
Bowtie2	(Langmead and Salzberg, 2012)	RRID:SCR_005476
MACS2	(Zhang et al., 2008)	RRID:SCR_013291
GenomicRanges	(Lawrence et al., 2013)	RRID:SCR_000025
deepTools2	(Ramírez et al., 2016)	RRID:SCR_016366
GREAT	(McLean et al., 2010)	RRID:SCR_005807
HOMER	(Heinz et al., 2010)	RRID:SCR_010881

References:

- Anders, S., Pyl, P. T. and Huber, W.** (2015). HTSeq--a Python framework to work with high-throughput sequencing data. *Bioinformatics* **31**, 166-169.
- Arner, E., Daub, C. O., Vitting-Seerup, K., Andersson, R., Lilje, B., Drablos, F., Lennartsson, A., Rönnérblad, M., Hrydziuszko, O., Vitezic, M., et al.** (2015). Gene regulation. Transcribed enhancers lead waves of coordinated transcription in transitioning mammalian cells. *Science (New York, N.Y.)* **347**, 1010-1014.
- Bolger, A. M., Lohse, M. and Usadel, B.** (2014). Trimmomatic: a flexible trimmer for Illumina sequence data. *Bioinformatics* **30**, 2114-2120.
- Dobin, A., Davis, C. A., Schlesinger, F., Drenkow, J., Zaleski, C., Jha, S., Batut, P., Chaisson, M. and Gingeras, T. R.** (2013). STAR: ultrafast universal RNA-seq aligner. *Bioinformatics* **29**, 15-21.
- Heinz, S., Benner, C., Spann, N., Bertolino, E., Lin, Y. C., Laslo, P., Cheng, J. X., Murre, C., Singh, H. and Glass, C. K.** (2010). Simple combinations of lineage-determining transcription factors prime cis-regulatory elements required for macrophage and B cell identities. *Molecular Cell* **38**, 576-589.
- Huang, D. W., Sherman, B. T., Tan, Q., Collins, J. R., Alvord, W. G., Roayaie, J., Stephens, R., Baseler, M. W., Lane, H. C. and Lempicki, R. A.** (2007). The DAVID Gene Functional Classification Tool: a novel biological module-centric algorithm to functionally analyze large gene lists. *Genome biology* **8**, R183-116.
- Langmead, B. and Salzberg, S. L.** (2012). Fast gapped-read alignment with Bowtie 2. *Nature Methods* **9**, 357-359.
- Lawrence, M., Huber, W., Pagès, H., Aboyoun, P., Carlson, M., Gentleman, R., Morgan, M. T. and Carey, V. J.** (2013). Software for computing and annotating genomic ranges. *PLoS computational biology* **9**, e1003118.
- McLean, C. Y., Bristor, D., Hiller, M., Clarke, S. L., Schaar, B. T., Lowe, C. B., Wenger, A. M. and Bejerano, G.** (2010). GREAT improves functional interpretation of cis-regulatory regions. *Nature Biotechnology* **28**, 495-501.
- Quaife-Ryan, G. A., Sim, C. B., Ziemann, M., Kaspi, A., Rafehi, H., Ramialison, M., El-Osta, A., Hudson, J. E. and Porrello, E. R.** (2017). Multicellular Transcriptional Analysis of Mammalian Heart Regeneration. *Circulation* **136**, 1123-1139.
- Ramírez, F., Ryan, D. P., Grüning, B., Bhardwaj, V., Kilpert, F., Richter, A. S., Heyne, S., Dündar, F. and Manke, T.** (2016). deepTools2: a next generation web server for deep-sequencing data analysis. *Nucleic acids research* **44**, W160-165.
- Robinson, M. D., McCarthy, D. J. and Smyth, G. K.** (2010). edgeR: a Bioconductor package for differential expression analysis of digital gene expression data. *Bioinformatics* **26**, 139-140.

Spurrell, C. H., Barozzi, I., Mannion, B. J., Blow, M. J., Fukuda-Yuzawa, Y., Afzal, S. Y., Akiyama, J. A., Afzal, V., Tran, S., Plajzer-Frick, I., et al. (2019). Genome-Wide Fetalization of Enhancer Architecture in Heart Disease. *bioRxiv*, 591362.

Visel, A., Blow, M. J., Li, Z., Zhang, T., Akiyama, J. A., Holt, A., Plajzer-Frick, I., Shoukry, M., Wright, C., Chen, F., et al. (2009). ChIP-seq accurately predicts tissue-specific activity of enhancers. *Nature* **457**, 854-858.

Ye, J., Coulouris, G., Zaretskaya, I., Cutcutache, I., Rozen, S. and Madden, T. L. (2012). Primer-BLAST: A tool to design target-specific primers for polymerase chain reaction. *BMC Bioinformatics* **13**, 134.

Zhang, Y., Liu, T., Meyer, C. A., Eeckhoute, J., Johnson, D. S., Bernstein, B. E., Nusbaum, C., Myers, R. M., Brown, M., Li, W., et al. (2008). Model-based analysis of ChIP-Seq (MACS). *Genome biology* **9**, R137.